Functional Hierarchy of the Human Neocortex from Cradle to Grave

Hoyt Patrick Taylor IV[1,✉], Kim-Han Thung[2,3], Khoi Minh Huynh[2,3], Weili Lin[2,3], Sahar Ahmad[2,3], & Pew-Thian Yap[2,3,✉]

[1]*Department of Computer Science, University of North Carolina, Chapel Hill, U.S.A.*
[2]*Department of Radiology, University of North Carolina, Chapel Hill, U.S.A.*
[3]*Biomedical Research Imaging Center, University of North Carolina, Chapel Hill, U.S.A.*

Recent evidence indicates that the organization of the human neocortex is underpinned by smooth spatial gradients of functional connectivity (FC). These gradients provide crucial insight into the relationship between the brain's topographic organization and the texture of human cognition. However, no studies to date have charted how intrinsic FC gradient architecture develops across the entire human lifespan. In this work, we model developmental trajectories of the three primary gradients of FC using a large, high-quality, and temporally-dense functional MRI dataset spanning from birth to 100 years of age. The gradient axes, denoted as sensorimotor-association (SA), visual-somatosensory (VS), and modulation-representation (MR), encode crucial hierarchical organizing principles of the brain in development and aging. By tracking their evolution throughout the human lifespan, we provide the first ever comprehensive low-dimensional normative reference of global FC hierarchical architecture. We observe significant age-related changes in global network features, with global markers of hierarchical organization increasing from birth to early adulthood and decreasing thereafter. During infancy and early childhood, FC organization is shaped by primary sensory processing, dense short-range connectivity, and immature association and control hierarchies. Functional differentiation of transmodal systems supported by long-range coupling drives a convergence toward adult-like FC organization during late childhood, while adolescence and early adulthood are marked by the expansion and refinement of SA and MR hierarchies. While gradient topographies remain stable during late adulthood and aging, we observe decreases in global gradient measures of FC differentiation and complexity from 30 to 100 years. Examining cortical microstructure gradients alongside our functional gradients, we observed that structure-function gradient coupling undergoes differential lifespan trajectories across multiple gradient axes.

Understanding how brain network organization changes across the human lifespan is a central and longstanding goal in neuroscience. Recent work has shown that functional connectivity is organized along a series of axes, which are realized as smoothly varying spatial patterns on the cortex[1]. These axes or "gradients" stratify cortical locations according to orthogonal connectivity features corresponding to fundamental information processing hierarchies[2]. Establishing a normative timeline of how the governing motifs of functional connectivity architecture develop in healthy individuals from cradle to grave is essential to a principled explanation of the onset, development, and timing of psychopathology[3]. Further, enumerating the lifespan trajectories of cortical regions with respect to global organizational motifs of the functional connectome provides rich insight into the topographic maturation of global information processing

✉ Corresponding authors: Hoyt Patrick Taylor IV (hptaylor@live.unc.edu) and Pew-Thian Yap (ptyap@med.unc.edu)

hierarchies that scaffold complex cognition.

Recent work in this vein has challenged the conventional strategy of monolithically categorizing the function of discrete brain regions or networks, instead suggesting that network architecture is best understood in terms of the topographic organization of hierarchical information processing motifs that smoothly vary as gradients across the cortex[2,4]. The most well-studied connectivity gradient is the canonical sensorimotor-association (SA) axis. Explaining the most variance in FC, the SA axis is anchored at one end by primary unimodal systems and at the other end by high-order association cortex coinciding with the default-mode network (DMN)[1,2]. Similarly, there are repeated observations that the gradient explaining the second most variance in FC is an axis spanning between visual and somatosensory cortex (the VS axis), smoothly partitioning cortical locations according to their preferential involvement in modality-specific processing [1,2]. Finally, many studies have identified a tertiary gradient of FC which is anchored at opposite ends by cortical regions preferentially involved in modulation (frontoparietal control and attention networks) versus regions involved in representation (default, sensory, and visual networks)[1,5,6].

Several studies have sought to characterize how one or more of these axes change during particular developmental periods, yielding observations that serve as a valuable foundation for establishing a multi-dimensional lifespan gradient atlas[7]. Xia et al.[8] demonstrated altered FC gradient ordering during infancy compared to healthy adults, with the visual-somatosensory (VS) axis explaining the most variance in FC, and an axis similar to the SA axis with important topographic differences constituting the secondary gradient of FC. Further, an age-based sliding window analysis of group-average FC gradients between 6 and 17 years found that convergence to the adult gradient ordering occurs during early adolescence, with higher-order association cortex undergoing more protracted gradient development than unimodal cortex[8]. Finally, one study analyzed the development of gradients during adulthood, finding that 3-dimensional gradient embeddings of canonical resting-state networks become increasingly dispersed during later adulthood, marking decreasing within-network coherence during aging[9]. While these works have contributed a valuable foundation for understanding the development of FC gradient architecture, there are no previous studies offering a cohesive analysis of gradient architecture from cradle to grave until now.

Concurrently, there is a vast body of non-gradient analyses of developmental changes in FC organization that provide invaluable context for gradient-based studies. Repeated observations demonstrate that spatially dispersed, high-order resting-state networks are weakly expressed during infancy and early childhood, with strong local connections in unimodal cortex dominating FC during early life[10–14]. During childhood, the basic substrates of complex cognition, including working memory, attention, self-referential thinking, and language ability, begin to emerge, necessitating the transition from a distinctly infant to an adult-like FC architecture. Graph-theoretic studies have established the importance of integration, segregation, and the modular architecture resulting from their interplay as being crucial to this transition, driving the emergence of higher-order systems including default and control networks which serve as the principal facilitators of representation and top-down executive control, respectively[15–17]. Importantly, such transmodal networks globally coordinate information processing and are cortically distributed. As a result, their emergence and strengthening during childhood is enabled by increases in long-range con-

nection density and strength, which mediate the transition from the highly local infant to global adult-like FC organization[18] by the end of childhood and beginning of adolescence.

Once adult-like FC organization has been established, the honing and expansion of cognitive capacities incurred by adolescence and early adulthood coincide with subtle refinements of this architecture[19]. In particular, fine tuning of the integration and segregation in high order default-mode, frontoparietal control, and attention networks increase during this period, leading to more pronounced information processing hierarchies[20,21]. During aging, degradation of the segregation-integration balance that scaffolds hierarchical FC architecture has been associated with cognitive decline[22–24]. Moreover, this period is characterized by global de-differentiation in FC that coincides with decreasing fluid intelligence and working memory.

Previous FC gradient studies provide useful insight into how gradient organization develops during particular developmental period, however none of these studies encapsulate the entire lifespan and their analysis methods and reporting vary significantly. We aim to address these shortcomings of the developmental FC gradient literature by analyzing functional MRI (fMRI) data of healthy individuals spanning from cradle to grave in a common unified framework. In this work, we sought to reconcile, augment, and unify previous developmental FC studies by harnessing the power of the FC gradient framework in combination with a large sample size, high-quality fMRI dataset. To this end, we developed a unified framework for charting the lifespan trajectories of well-studied and validated axes of FC organization. We then used this lifespan atlas of global FC architecture to characterize changes in the topography of individual gradient axes, global features, and multi-dimensional embedding they collectively constitute.

RESULTS

Our analysis aimed to chart changes in global intrinsic FC organization across the human lifespan. To this end, we computed low dimensional representations of the vertex-wise functional connectivity data of 2,735 subjects with ages spanning from 16 days to 100 years using the diffusion map embedding approach[1] (Figure 1). When applied to FC data, diffusion embedding has been demonstrated to yield smooth patterns of variation in connectivity, referred to as FC "gradients". In tandem, diffusion embeddings preserve global connectivity relationships in the underlying FC graph, providing a low-dimensional approximation of the global organizing geometry of the functional connectome.

We developed a framework that allows for joint analysis of the FC gradients for all subjects in a common space. First, we computed a template gradient set based on the principal components of variation across all gradients. These template gradients corresponded to well-studied cortical gradients spanning respectively between cortical locations implicated in sensorimotor-association (SA), visual-somatosensory (VS), and modulation-representation (MR). Together, these axes define the embedding space in which we carried out the remainder of our analysis. We proceeded by aligning all individual subject gradients to this template space using Procrustes alignment[25], after which the gradient value at each vertex for all subjects measures the same connectivity characteristic. Finally, by fitting generalized additive mixed models (GAMMs)[26] to gradient value at each cortical surface vertex versus age, we obtain a population-

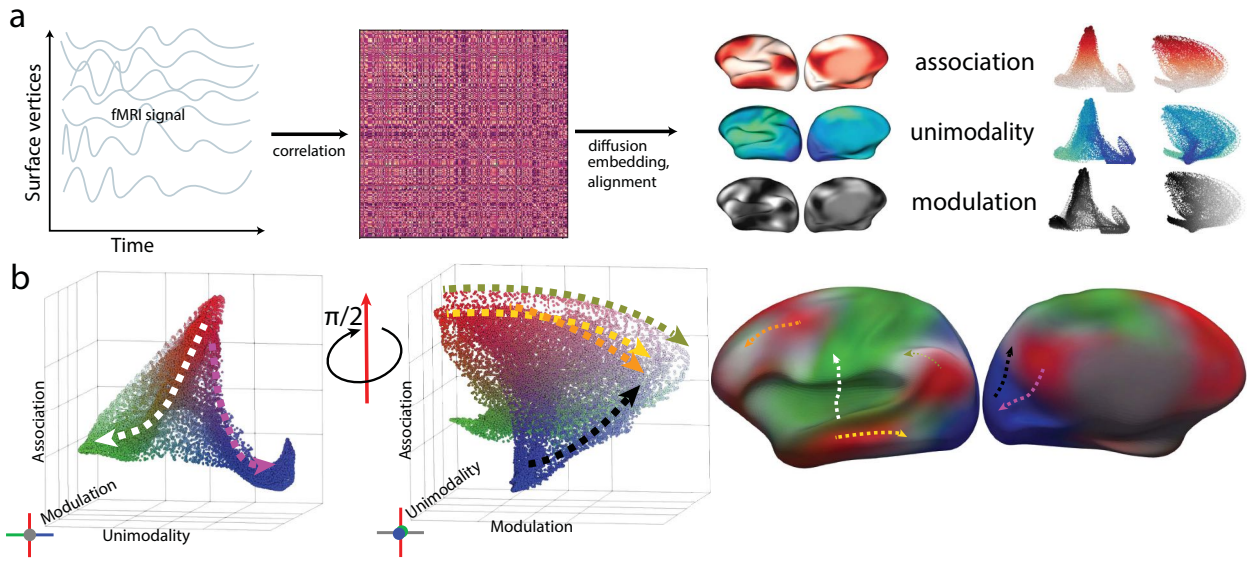

Fig. 1 | Overview of gradient manifold computation and its interpretation. **a**, For each subject, fMRI signal is mapped to the cortical surface and a functional connectivity (FC) matrix is computed via Pearson correlation coefficient. Individual subject FC gradients are obtained via diffusion embedding applied to the FC matrix, and are aligned to the template gradient axes of interest: sensory-association (SA) , visual-somatosensory (VS), and modulation-representation (MR). Respectively, these axes differentiate cortical locations by their implication in association (red), their degree of unimodality in either visual (blue) or somatomotor (green) domains, and their propensity to engage in top-down modulation (white). **b**, The taxonomy of the adult gradient manifold in the embedding space (left) and the cortical surface (right) with a unified color map that combines the three used in **a**. Several paths along the gradient manifold are displayed with corresponding color-coded paths along the cortical surface, demonstrating the cortical realization of hierarchies enumerated by the gradient manifold.

level estimate of the trajectory of these aligned gradient values across the entire lifespan.

Our lifespan gradient fit provides the first ever comprehensive dynamic atlas of global FC organization from cradle to grave. Age-related changes in the cortical topography of each gradient provide insight into the spatial realization of three crucial organizational hierarchies on the human cortex. Simultaneously, the 3 dimensional gradient embedding reveals how the interrelationships between these hierarchies develop from birth to death. More specifically, the position of a vertex in the lifespan gradient embedding at a given age encodes its position with respect to the three principal axes of FC organization, giving a detailed description of that vertex's connectivity characteristics. Our result provides a temporally dense and spatially detailed normative reference of how these crucial information processing motifs evolve with respect to cortical locations.

Changes in gradient topography are concentrated in infancy and early childhood. A central objective of this study was to characterize how the cortical topography of the sensorimotor-association (SA), visual-somatosensory (VS), and modulation-representation (MR) axes vary with age. To this end, we analyzed our vertex-wise GAMMs of gradient values mapped to the cor-

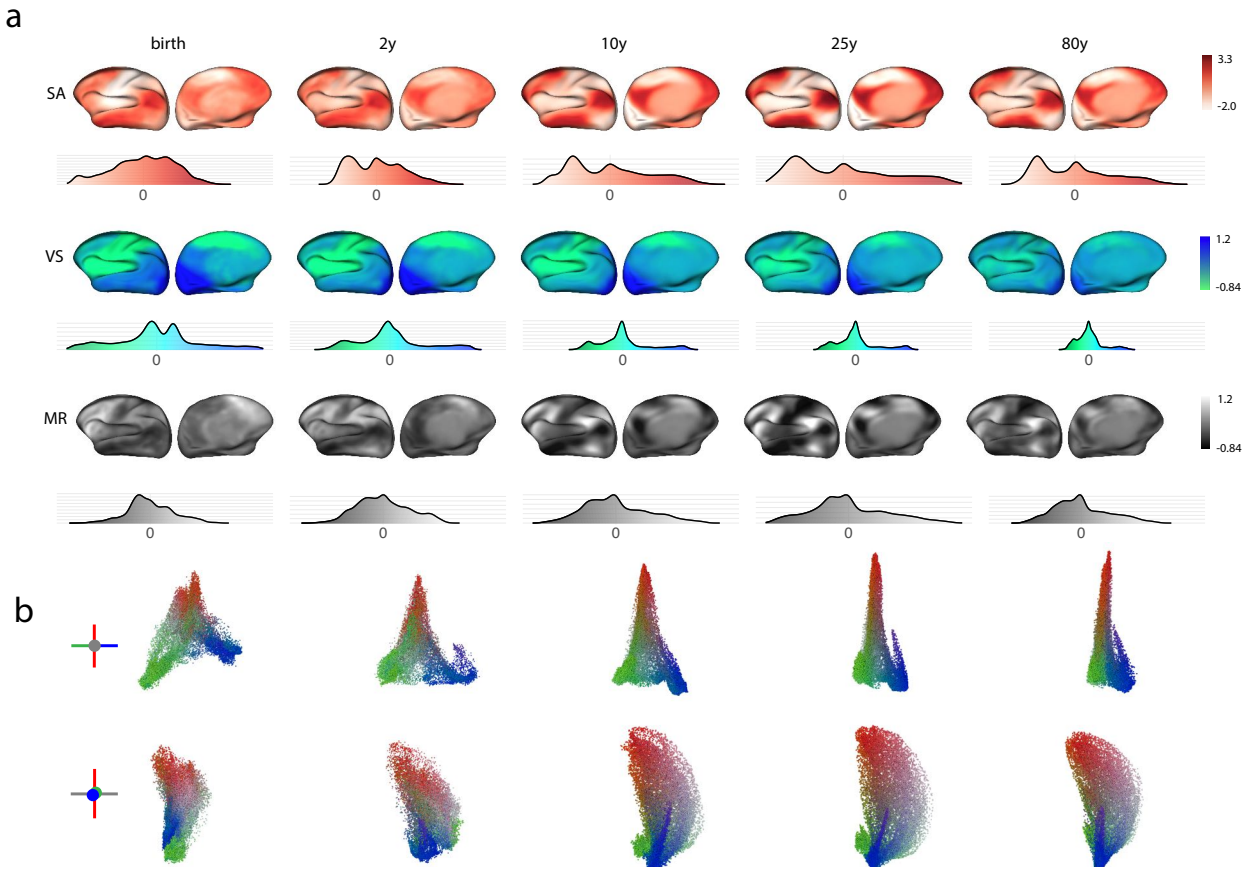

Fig. 2 | Gradient organization from cradle to grave. Sensory-association (SA), visual-somatosensory (VS), and modulation-representation (MR) gradients of FC undergo differential development across the human lifespan. **a**, GAMM fits of FC gradient value are plotted on the cortical surface with density plots displaying gradient value distribution at selected timepoints. **b**, Embedding plots given by gradient GAMM fits in SA-VS plane (top) and SA-MR plane (bottom).

tical surface (Figure 1a). The cortical topography of each gradient provides crucial insight into the spatial realization of critical patterns of variation in connectivity, while the distribution of values for each gradient details the hierarchical architecture of its corresponding connectivity characteristic. Crucially, our results allow us to examine the smooth temporal evolution of the principal gradients of FC across the human lifespan for the first time ever. Gradient value density plots (Figure 2) show this distribution and allow for characterization of global changes in each gradient across the lifespan. Peaks in gradient value density plots arise when many vertices share the same FC profile with respect to a gradient, whereas uniform, widespread density distributions indicate highly heterogeneous or stratified FC. Notably, gradient topography changes most significantly during the first 4 years of life, consistent with observations that infancy and early childhood represent critical periods for the development of large-scale adult-like network architecture[12,14,27–29].

We also quantitatively assessed the significance of age-related change in gradient value across the cortex on a region-wise basis by fitting GAMMs (6 smooth spline terms, subject ID

and cohort treated as random effects) to mean gradient value within each region in the Schaefer 400 region parcelletion[30]. SA gradient value varied significantly across the lifespan in the majority of cortical regions ($p_{\text{FDR}} < 0.05$ for 90% of regions), with the strongest age-related changes concentrated in somatosensory and default-mode parietal cortices. VS gradient value also varied significantly for a slightly greater proportion of cortical regions ($p_{\text{FDR}} < 0.05$ for 95% of regions), with fits of highest significance occurring in visual and somatosensory cortex. Age-related changes in MR gradient value were similarly significant across cortical regions ($p_{\text{FDR}} < 0.05$ for 90% of regions), with maximal significance occurring in control-oriented parietal and frontal cortex. We observed significant non-linearity in the lifespan trajectory of SA and MR gradient value across most cortical regions, with maximal lifespan fluctuation taking place in the transmodal association cortices that lie at the respective association and modulation poles of these gradients. In contrast, VS trajectories were more linear with respect to age.

The mature SA axis describes the principal organizing motif of functional connectivity, stratifying cortical locations according to their position along a hierarchy spanning from primary sensory regions to heteromodal association cortex[1]. In adults, we observe homogeneous values at the unimodal (negative) end of this axis and highly stratified values on the association (positive) pole (Figure 2a, SA density plot for 25 years). This is further evidenced by smoothly decreasing SA values emanating from the highly localized positive focal points (dark red) and homogeneous negative values (white) in unimodal cortices (Figure 2a, SA surface plots for 25 years). Between mid adolescence and old age, the cortical topography and heavy-tailed distribution of the SA axis remain constant, indicating that the spatial layout of this hierarchy is established during infancy, childhood, and early adolescence.

During early life, SA organization is distinct from that of adulthood, with very little stratification among cortical regions on its positive association pole and relatively greater stratification on its unimodal negative pole. The first two timepoints (birth and 2 years) in Figure 2a illustrate this difference, with homogenous positive (red) values on the cortical surface, steep falloff in SA value density on the positive side, and more gradual falloff in value density on the negative side. These distinctive features of the SA axis during early life underscore the absence of well-ordered sensory-association hierarchy and further indicate that FC organization during this period is dominated by unimodal processing and short-range connectivity. Figure S1 illustrates the immature and distinct topography of the SA axis during infancy, while Figure S2 displays the convergence of SA topography to its mature form that plays out between 2 and 6 years.

The transition from a highly local and unimodally driven architecture to the stratified hierarchical architecture of the mature SA axis takes place between 2 and 10 years of age (Figure 2a, SA axis). During this period, we observe significant focal tuning of positive peaks reflected by an increasingly heavy-tailed SA value distribution. This change is realized on the cortical surface as increasingly localized positive (red) peaks that converge towards the canonical loci of the default mode network. These shifts coincide with the development and crystallization of crucial aspects of identity, cognitive ability, and personality that take place during this critical period[12,19,21,31,32].

Like the SA axis, the mature modulation-representation (MR) axis enumerates an information processing hierarchy whose apex is comprised by spatially distributed heteromodal cortical regions. Whereas regions atop the SA axis are central to the DMN, the modulation pole of the

MR axis is comprised of core constituents of the frontoparietal control network (FPC) and attention networks[6,33]. Like the SA axis, the positive pole of the MR axis is highly stratified, however its negative pole is also highly stratified, exhibiting strong focal tuning of its representation loci (Figure 2a, 25 years, MR, black). A sharp peak in the center of the MR distribution in combination with gradually decaying tails at both poles indicate that only a small number of brain regions are recruited strictly for modulation or for representation. Rather, the plurality of cortical regions occupy some middle ground between these extremes. As a result, the spatially dispersed positive and negative poles of the MR axis are highly localized.

During early life, the MR axis very weakly resembles its mature form (Figure 2a, MR, birth + 2 years). Figure S1 and Figure S2 illustrate the maturation of the MR axis during early life, exhibiting the least similarity to its mature form among our three gradients of interest. Neither positive modulation or negative representation poles are highly localized, with relatively low degrees of stratification towards either extreme. Between birth and 2 years, superior parietal regions encompassing portions of the mature dorsal attention network as well as inferior parietal lobule constituting loci of the salience and frontoparietal control networks move towards the positive modulation pole, however there is still weak stratification at 2 years. Between 2 and 10 years, adult-like MR topography emerges with increasing stratification of both poles and focal tuning of peaks (Figure S2), indicating that this period is critical to the development of the differentiation between control-oriented and representation-oriented cortical regions. The MR axis undergoes further refinement between 10 and 25 years, with the somatosensory cortex occupying an increasingly negative (representation-oriented) position, and peaks in the frontal cortex shifting towards the positive (modulation) pole (Figure S3). This prolonged developmental trajectory is consistent with repeated observations that development of executive function and control is protracted and persists into early adulthood[34,35].

In contrast to the high-order information processing hierarchies corresponding to the SA and MR axes and the complex topographic development they undergo, the VS axis differentiates brain regions with respect to preferential involvement in the two primary unimodal processing domains and has stable cortical topography throughout the lifespan. Stratification along the VS axis is maximal during early life (0–2 years), indicating that the distinction between unimodal sensory processing modalities is dominant in shaping FC organization during this period. Interestingly, the positive (visual) and negative (somatosensory) poles of the VS axis become more spatially localized between birth and 10 years, with more abrupt spatial transitions in gradient value surrounding unimodal cortices. Simultaneously, the global range and the stratification of extreme positive and negative values of the VS axis decrease during this period. Together, these trends signify a global decrease in modality-specific processing and an increase in the homogeneity of FC in primary unimodal cortex. This is further underscored by increasing concentration of values on the negative (unimodal) pole of the SA axis also observed during this period. Together, these observations suggest that functional specialization of primary sensory and visual cortices takes place between birth and early childhood and that the strong local connections present in these systems play the largest role in shaping the global architecture of the functional connectome during early life.

Global measures of FC gradient organization exhibit non-linear changes across the lifespan. We observe significant non-linear developmental trajectories in global properties of all three of

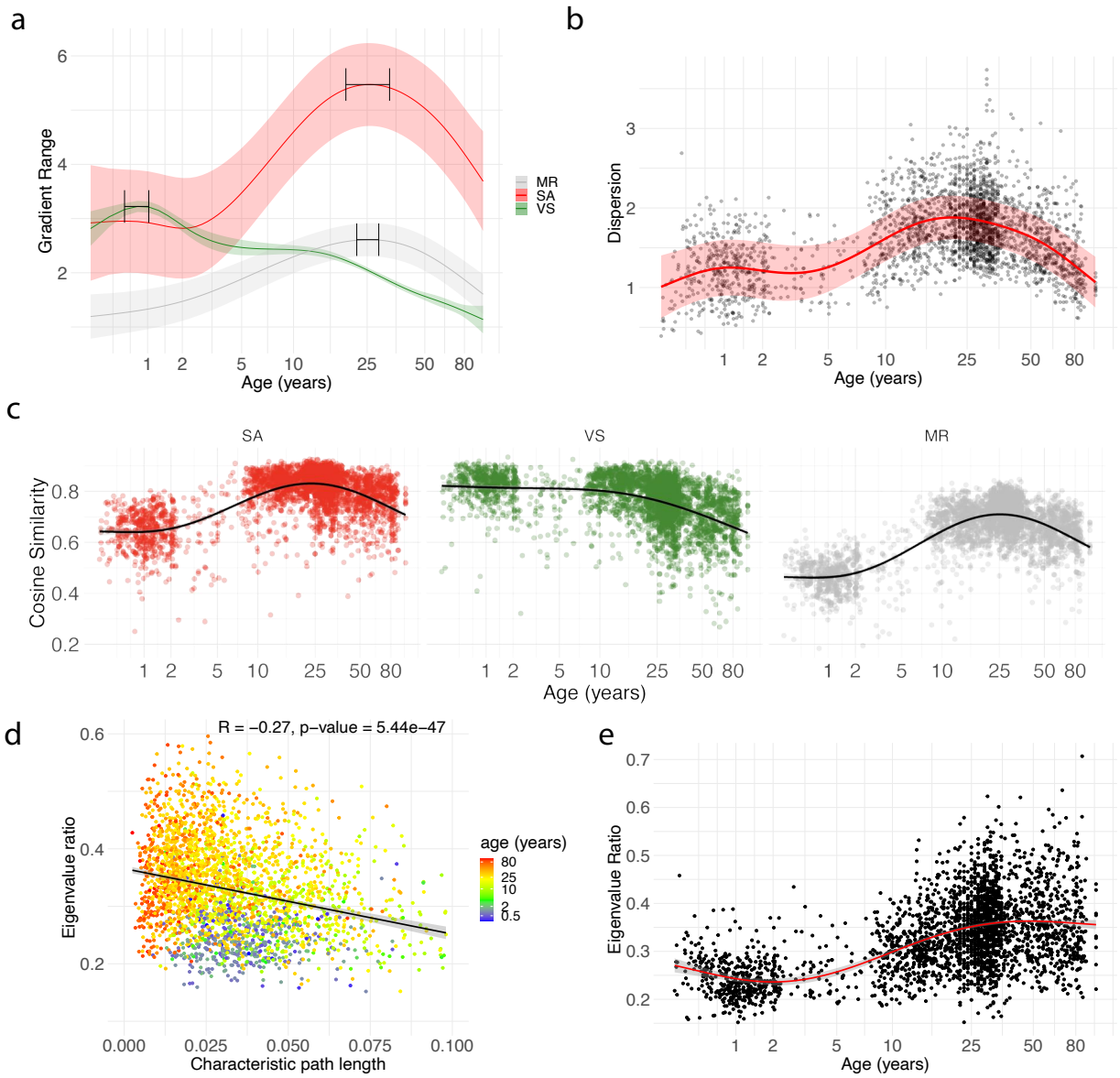

Fig. 3 | Global gradient metrics denote changes in hierarchical FC architecture across the lifespan. **a**, Inter-vigintile gradient range versus age (log scale) with GAMM fits for SA, VS, and MR axes. **b**, Gradient dispersion versus age with GAMM fit. **c**, Cosine similarity between individual subject gradients and template gradient set used for alignment. **d**, Characteristic path length versus eigenvalue ratio (the first diffusion embedding eigenvalue divided by the sum of all eigenvalues). **e**, Eigenvalue ratio versus age with GAMM fit.

our gradient axes and the 3-dimensional embedding they constitute. To measure the global expression of a gradient, we compute gradient range as the inter-vigintile range (5th percentile to 95th percentile), robustly quantifying the prominence of its corresponding connectivity motif. We fit GAMMs to the range of SA, VS, and MR axes and observe significant non-linear developmental trajectories across the lifespan for each of them, indicating that FC organization undergoes complex reorganization in multiple hierarchical dimensions from cradle to grave (Figure 3). Both SA and MR axes undergo gradual expansion throughout infancy, childhood, and adolescence. The scale of the SA axis reaches a pronounced peak during early adulthood (25.7 years, 95% CI 19.2–32.5 years). Similarly, the range of the MR axis increases monotonically throughout infancy, childhood, and adolescence, reaching a more protracted and smooth peak during early adulthood (25.52 years, 95% CI 22.0–28.8 years). During early adulthood, the range of the SA and MR axes are stable, however the SA axis undergoes more rapid contraction during mid and late adulthood compared to the MR axis, which only contracts modestly. Both SA and MR axes exhibit inverted U-shaped development previously observed in lifespan FC development[36]. In contrast, the VS axis, which differentiates between the primary unimodal processing centers, increases rapidly during infancy and early childhood, reaching its maximum range at 0.77 years (95% CI 0.27-1.8 years), undergoing gradual contraction throughout the remainder of the lifespan.

Expansion of the transmodal SA and MR gradients throughout development is consistent with abundant evidence that heteromodal association and modulatory attention and executive cortex have protracted maturation[34,37–39]. As gradient range measures the differentiation in FC between cortical locations at each pole of the gradient, the expansion of the SA axis signifies increasing functional dissimilarity between default-mode association cortex (Figure 1a, top right cortical surface, red) and primary unimodal cortex (Figure 1a middle right cortical surface, blue and green). In turn, expansion of the MR axis marks an increasing contrast in the connectivity profiles of modulation-implicated (frontoparietal control and attention) cortex, and representation-implicated systems (default, sensory, visual, and limbic). Importantly, this expansion is modest during infancy and early childhood and becomes more rapid during later childhood and adolescence, indicating that the unfurling of these crucial organizing motifs of the functional connectome coincides with the transition from childhood to adulthood (Figure 3a, red). The VS gradient displays highly divergent global development compared to the SA and MR axes. Namely, the range of the VS axis peaks during infancy (0.77 years, 95% CI 0.27-1.8 years), followed by significant decline thereafter. This trend is consistent with previous studies that observe a decrease in the variance explained by the VS axis[29] as well as studies showing a transition from local to long-range FC organization throughout development[18].

We also studied how the dispersion of vertices in our 3-dimensional embedding space changed throughout the lifespan by computing gradient dispersion, the average embedding distance between each vertex and the embedding centroid for each subject. Because Euclidean distance in the diffusion embedding space approximates geodesic distance in the underlying FC matrix, gradient dispersion provides a measure of global FC differentiation with respect to the SA, VS, and MR axes. High dispersion values indicate globally heterogeneous FC profiles, while lower dispersion values correspond to lower cortex-wide diversity in FC profiles. It is important to note that dispersion provides a scalar summary of the spread of vertices in all three gradient dimensions despite the differential contribution of each axis to the Euclidean distances in embedding space. With this in mind, dispersion should be interpreted in combination with information

about the relative scale of each gradient axis (Figure 3a).

After computing mean dispersion for each subject, we fit a GAMM to model the lifespan trajectory of dispersion with respect to age (Figure 3). Age was treated as a smooth term modeled using smooth splines with $k = 4$ basis functions, and subject ID and cohort ID were treated as random effects. Figure 3b shows a modest increase in dispersion during infancy (0–1 year) and stable dispersion during early childhood (1–4 years) coinciding with commensurate increase in SA axis range and decrease in VS axis range (Figure 3a). Dispersion increases rapidly between 5 and 21.3 years (95% CI 19.3-23.0 years), remains relatively stable during mid adulthood (23–40 years), and decreases steadily thereafter. Increases in dispersion throughout late childhood, adolescence, and early adulthood coincide with significant expansion of the SA and MR axes, reflecting a global increase in FC differentiation, particularly with respect to high-order information processing hierarchies. Declining dispersion during later adulthood reflects decreasing global connectivity differentiation in tandem with reduction in the range of all three gradient axes, indicating that FC profiles become more globally homogeneous during aging. This nonlinear trajectory serves as a normative reference for the global differentiation of FC with respect to the first three hierarchical axes of organization across the lifespan.

To further substantiate our gradient-based global measures of FC organization, we computed a number of graph-theoretical metrics from the FC matrices underlying our gradients and fit GAMM's versus age to model their lifespan trajectories. These fits are displayed in Figure S4, with metrics including the mean, variance, and skewness of the FC degree distribution, characteristic path length, mean vertex eccentricity, graph radius, assortativity, mean clustering coefficient, and modularity [40]. In keeping with our observations that gradient topography reaches its stable, mature form at approximately 10 years, we also observe peaks during early adolescence in a number of graph theoretical metrics including degree, characteristic path length, eccentricity, and clustering coefficient. It is particularly interesting that peaks in global gradient measures including dispersion and gradient range do not coincide with mean FC degree and characteristic path length, which instead peak in tandem with the stabilization of gradient topography. These results suggest that the establishment of adult-like gradient topography coincides with the attainment of a maximally connected functional connectome.

Comparison of FC gradients across subjects required alignment of individual gradient sets to a template gradient set. This template, computed via PCA applied to the individual gradients of all subjects, consisted of the SA, VS, and MR axes. While these three gradient axes represent the most prevalent FC motifs across the human lifespan, the topography, ordering, and scale of individual gradients varies significantly. To probe how the topography of individual gradients varied with respect to our canonical template gradients, we computed the cosine similarity between the aligned gradients of each individual and the corresponding template gradient. Figure 3c displays template cosine similarity for all subjects versus age with GAMMs fit analogously to dispersion. Critically, topographic similarity of the SA and MR axes to the canonical template show highly similar lifespan trends: similarity to the template is constant during infancy (0–2 years), increases monotonically between 2 and 25 years (peaks at 24.7 years, 95% CI 16.3–29.1 years), and declines steadily thereafter. It is notable that the transmodal SA and MR axes exhibit analogous lifespan topographic organizational trends. Further, significantly declining cosine similarity of the MR axis and moderate decline of the SA axis during adulthood and aging (25+ years) indicate that

with age, SA and MR topography become more individualized and idiosyncratic. The topographic similarity of the VS axis of individuals to our canonical template VS axis exhibits very slow decline throughout the entire lifespan. During infancy, topographic consistency of the VS axis is at its lifespan maximum, indicating that there is lower inter-subject variation in the VS axis during this period. The steady decline in the VS axis topographic similarity indicates that with age, this connectivity motif becomes increasingly individualized in tandem with its decreasing salience as an organizing axis of FC as demonstrated by declining gradient range (Figure 3a).

Resting-state networks undergo significant gradient reorganization throughout the lifespan. Previous studies have demonstrated that canonical resting-state networks are stratified along the primary FC gradients[1,41]. In tandem, there is mounting evidence that brain development plays out along cortical gradients including the SA axis[37], with unimodal networks achieving maturity far earlier than limbic, attention, and association networks[31,42,43]. We investigated the reconfiguration of canonical resting-state networks in our aligned gradient embedding space using Yeo et al.'s 7-network connectivity-based network parcellation[44]. We first analyzed network trajectories in our embedding space by computing the median gradient value in each network and each gradient for all subjects. Then, to assess the lifespan trajectory of networks along each gradient axis, we fitted GAMMs to the median gradient value in each network for each gradient separately. Age was treated as a smooth fixed effect and subject ID and dataset cohort were treated as random effects. Importantly, we observe differential trajectories of median gradient value across networks and across axes (Figure 4a), indicating that networks undergo complex maturational timing with respect to the principal axes of FC organization.

The expansion of the SA axis during development and its contraction during aging mediate the lifespan changes in resting-state network configuration along this unimodal-to-transmodal axis. Namely, the positions of default, control, and limbic networks along the SA axis increase modestly between birth and 10 years, increase rapidly between 10 and 30 years, and decline steadily for the remainder of the lifespan (Figure 4a, left). Conversely, the salience/ventral attention, dorsal attention, and visual networks move down the SA axis gradually between birth and 25 years, and move to a more central position thereafter. Migration towards the negative pole of the SA axis indicates that these networks become more closely integrated with the unimodal "base" of the sensory-association information processing hierarchy. Interestingly, the somatomotor network begins at an extreme negative position along the SA axis, moves to a more central (less unimodal) position between birth and 3 years, and then converges to the trajectory observed in the attention and visual networks (Figure 4c). This differential trajectory of the somatomotor network during early development is potentially explained by consideration of the topographic reorganization of the SA axis during this period, wherein the negative pole is initially strongly concentrated in the somatomotor cortex and gradually equalizes with the visual system thereafter (Figure 2a).

The VS axis discriminates brain locations according to preferential involvement in visual versus somatosensory processing streams. Thus, heteromodal networks including default, control, limbic, and dorsal attention occupy central positions on the VS axis throughout the lifespan (Figure 4c). Visual and somatomotor networks occupy the extreme positive and negative poles of the VS axis throughout the lifespan, with the salience/ventral attention network situated on the somatomotor side of the axis. This positioning of the salience/ventral attention network is strik-

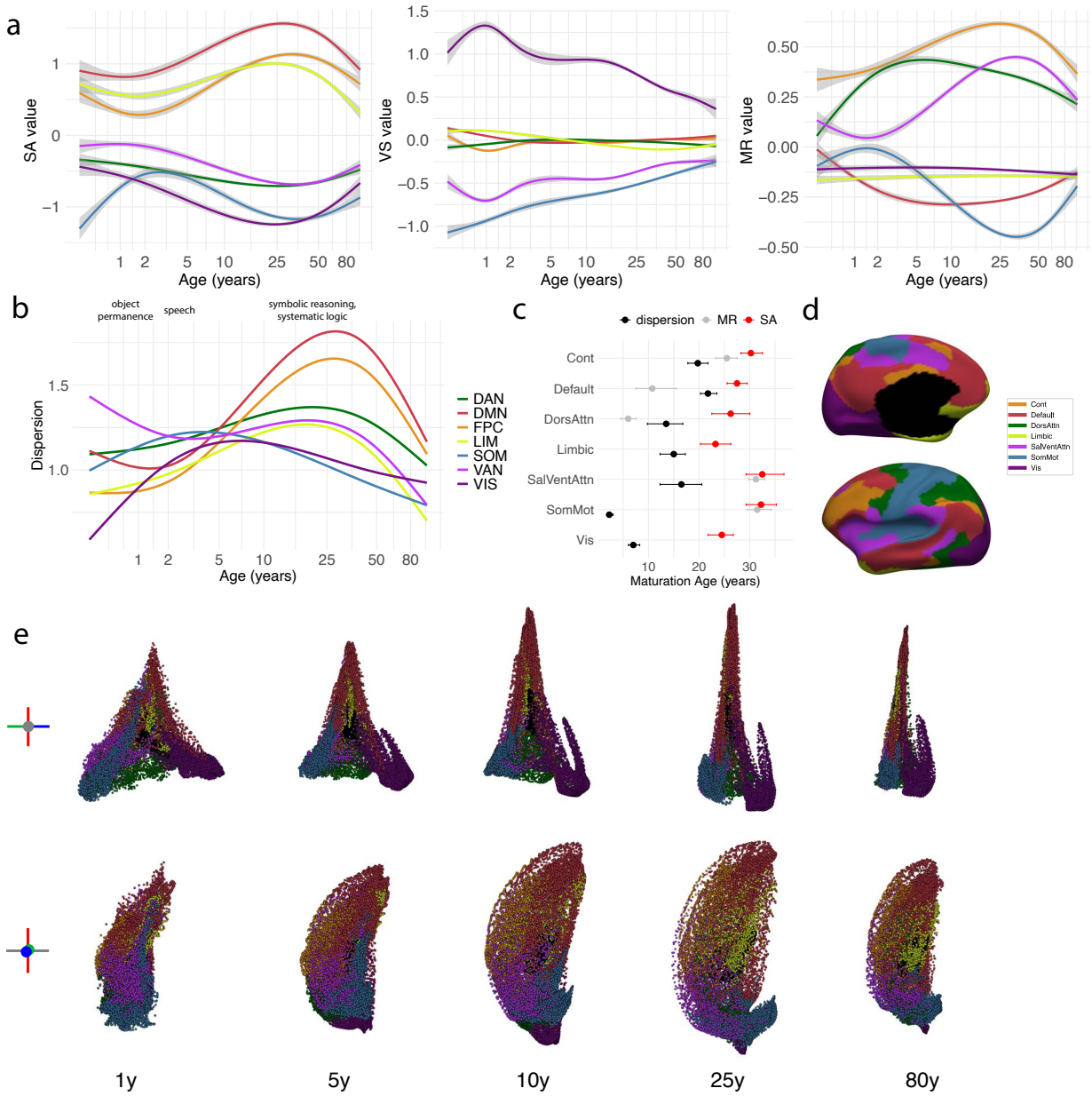

Fig. 4 | Lifespan development of functional gradients with respect to canonical resting-state networks across the lifespan. **a**, GAMM fits of mean gradient value versus age within each network parcel for SA, VS, and MR axes. **b**, GAMM fit of within-network dispersion versus age, computed as the mean squared Euclidean distance between each vertex's coordinate in the SA-VS-MR gradient embedding space and the network centroid. **c**, Maturation age of network-wise gradient value and dispersion. For gradient value, maturation age is taken as the timepoint at which the GAMM fit for a particular network along a particular gradient reaches its most extreme value along that gradient. The VS axis is excluded due to its contraction throughout the lifespan. For dispersion, maturation age is treated as the age at which maximum dispersion occurs for a network. **d**, Yeo 7-network[44] parcellation plotted on the cortical surface. **e**, GAMM-fitted gradient embedding plots colored using the Yeo 7-network parcellation scheme at selected timepoints across the lifespan viewed from the SA-VS plane (top) and the SA-MR plane (bottom).

ing, indicating dominance of somatomotor processing in top-down attention modulation. During infancy, the somatomotor and visual networks are maximally distant on the VS axis (Figure 4a, middle). Notably, the median VS coordinate of somatomotor vertices takes on its most extreme negative position at birth and trends towards a more central position throughout the duration of the lifespan. In contrast, the visual network moves to an increasingly positive position on the VS axis between birth and 1 year (95% CI 10.2–13.7 months), reflecting increasing unimodal specialization of visual processing during early life. The salience/ventral attention network, which contains crucial areas of premotor cortex, also moves to a more extreme negative position on the VS axis between birth and 1 year (95% CI 11.1–13.2 months), indicating an increase in preferential involvement in somatomotor unimodal processing during this period. The networks occupying the poles of the VS axis (visual, somatomotor, and salience/ventral attention networks) rapidly move towards the center of the VS axis between 1 and 4 years, plateau between 4 and 10 years, and contract towards a central position steadily throughout the remainder of the lifespan in tandem with the global contraction of the VS axis as indicated by its declining gradient range (Figure 3a).

Network centroids along the MR axis exhibit the most complex lifespan dynamics, with varied maturational timings and developmental profiles across multiple networks (Figure 4c). The MR axis differentiates brain regions with respect to their preferential involvement in top-down modulation versus representation. It therefor stands to reason that control and attention networks occupy the modulation pole and default, limbic, and unimodal networks occupy the representation pole. Default and control networks become increasingly separated on the MR axis with age. However, the default mode network reaches its mature extreme position during early adolescence (10 years, 95% CI 6.1–13.2 years), whereas the control network moves to an increasingly positive position throughout adolescence until peaking at 28 years (95% CI 27.7–36.4 years). After 30 years, both default and control networks move to more central positions, coinciding with the contraction of the MR axis during this period (Figure 2b). Dorsal and ventral attention networks undergo differential development along the MR axis, with their maximum positions reached at 4 years (95% CI 3.6–4.4 years) and 30 years (95% CI 29.7–35.0 years), respectively.

Interactions between resting-state networks in gradient space track developmental refinement of FC organization. Our analysis of changes in dispersion and gradient value within resting-state networks demonstrated that gradient reorganization is nonlinear across the lifespan and heterogeneous across networks. Further, inspection of our GAMM fits of gradient value revealed that the 3-dimensional distributions of network nodes in embedding space change significantly across the lifespan. To characterize these changes and the interaction between networks in greater detail, we analyzed the pairwise distance distributions between vertices in each pair of networks. Previous studies have computed "between-network dispersion" by first taking the mean embedding coordinate of vertices within each network and then computing the Euclidean distance between these network centroids[9]. While this is a good first-order approximation, it discards rich information about the shape and spread of vertices within each network. Instead, we define the between-network dispersion as the median distance between all pairwise Euclidean distances between vertices in two networks and normalize this quantity by the global dispersion of the embedding. We computed between-network dispersion for each network pair in each subject's aligned gradient embedding, then fitted GAMMs versus age for each network pair with age

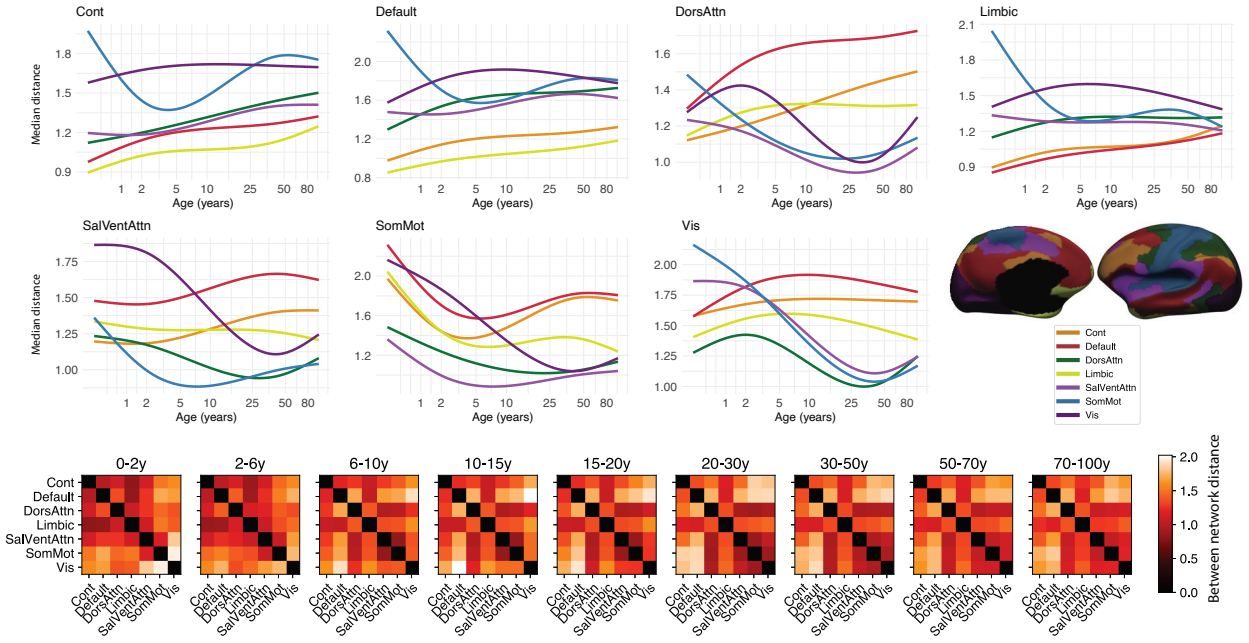

Fig. 5 | GAMM fits of median gradient embedding distance between resting-state networks. Larger distances correspond to higher levels of functional differentiation and segregation. Small distances indicate functional similarity and integration. (Top) each plot displays the lifespan GAMM fit of the median Euclidean distance in the SA-VS-MR gradient embedding space between vertices in the title network and vertices in each other network. (Bottom) Matrix plots of average network-network mean embedding distance in selected temporal windows, with lighter values denoting larger distance.

treated as a smooth term and subject ID and cohort included as random effects (Figure 5).

Our relative between-network dispersion metric can be interpreted as a measure of between-network segregation, with higher values indicating segregation between two networks and lower values indicating increased integration. With this in mind, Figure 5 illustrates the lifespan changes in integration/segregation for each pair of resting-state networks. We observe a period of rapid changes in between network dispersion between birth and 2 years, with increasing dispersion between visual-default, visual-control, and visual-dorsal attention and decreasing dispersion between somatomotor-default and somatomotor-control. These rapid reconfigurations during early life are consistent with evidence that infancy represents a critical period for the simultaneous proliferation and pruning of functional connections[45,46]. From birth to 5 years, the dorsal attention network becomes increasingly dispersed relative to the default network after which there is little change in their interaction. Simultaneously, dorsal attention and control networks become increasingly dispersed throughout the lifespan, indicating progressive segregation between these systems which is persistent throughout development. Interestingly, the dispersion between default and control networks does not increase monotonically throughout development, but instead increases between birth and 5 years and declines modestly between 5 and 30 years. This result indicates that infancy and early childhood are critical for the differentiation between these high-order systems and that the development of these networks from 5 to 30 years is driven

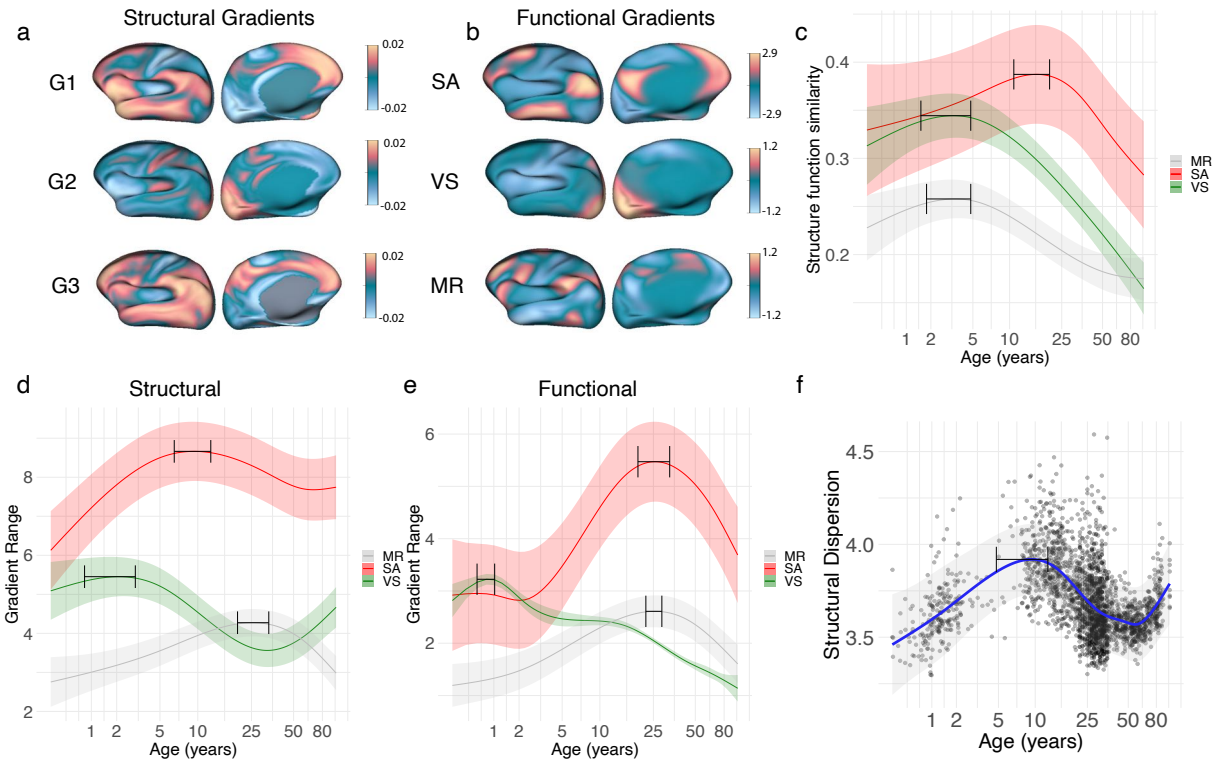

Fig. 6 | Analysis of structural gradients based on cortical thickness, myelination, and microstructural indices. **a**, Surface plots of group-level structural gradients aligned to functional gradient template. **b**, GAMM fits of structure-function coupling between individual structural gradients and individual functional gradients after Procrustes alignement for SA, VS, and MR axes. **c**, Dispersion of structural gradients from birth to death with GAMM fit and 95 % CI for maximum value.

by changes in the scale of our gradient axes themselves rather than changes in the position of default and control networks relative to those axes. This reasoning is bolstered by our observations that gradient topography is largely stable after 5 years, with lifespan changes during childhood, adolescence, and adulthood restricted to gradient range rather than by shifting topography.

Structure-function coupling undergoes nonlinear and divergent lifespan evolution across multiple cortical hierarchies. We also sought to probe the relationships between morphological and microstructural cortical features and our FC gradients across the human lifespan. To this end, we computed structural gradients using cortical thickness, myelination, intra-cellular volume fraction, extra-cellular volume fraction, intra-soma volume fraction, fractional anisotropy, mean diffusivity, microscopic fractional anisotropy, microscopic mean diffusivity, microscopic anisotropy index, and orientation coherence index as a feature space from which structural affinity matrices were computed using pairwise Pearson correlation. For each subject, we then computed structural gradients analogously to our functional gradients, yielding a set of axes of structural organization for all subjects. We then aligned the structural gradient embeddings of each subject to their corresponding functional gradients which were previously aligned to our lifespan functional gradient template consisting of the SA, VS, and MR axes. We observed modest to-

pographical similarity between structural gradients and individual SA, VS, and MR functional gradients, with an average spatial correlation between structural and functional gradient counterparts of ρ=0.34 for the SA axis, ρ=0.27 for the VS axis, and ρ=0.21 for the MR axis. These modest spatial correlations suggests that the principal axes of functional organization do not strongly coincide topographically with underlying patterns of variation in cortical microstructure. To assess lifespan changes in the similarity between our structural and functional gradients, we computed cosine similarity between aligned structural and functional gradients for each subject and subsequently fitted GAMMs to obtain lifespan trajectories of axis-specific structure-function coupling (Figure 6b).

Not surprisingly, our structural gradients are topographically distinct from our functional gradients even after Procrustes alignment (Figure 6a). Qualitatively, structural and functional counterparts of the SA axis are similar, while the VS-aligned structural gradient exhibits large differences from the functional VS axis. Specifically, while the visual cortex is positive in both the functional and structural VS axes, the somatosensory cortex does not reside at the negative pole in the VS-aligned structural gradient. This indicates that differences in cortical microstructure between the visual and somatosensory systems do not topographically coincide with the functional VS axis. The MR-aligned structural gradient also diverges from its functional counterpart, with far less spatial localization in its positive pole. It further lacks the negative pole in DMN loci in the inferior parietal lobule exhibited in the functional MR axis. Together, these results suggest that there is strong microstructural underpinning of the SA axis, but far weaker orthogonal gradients of cortical microstructure underpinning the secondary and tertiary VS and MR axes.

Developmentally, the topographic similarity between these structural gradients and their functional counterparts undergo significant lifespan evolution (Figure 6c). Structure-function gradient similarity increases across all three axes during infancy and childhood, indicating that the functional differentiation observed during this period coincides with commensurate differentiation in cortical microstructure. Coupling peaks for the VS axis at 2.8 years (95% CI 1.7-4.9 years) and for the MR axis at 3.1 years (95% CI 1.9-4.9 years) and declines monotonically for both axes thereafter. In contrast, SA structure-function coupling increases from birth until 13.2 years (95% CI 10.2-20.1 years), indicating that the topographic refinement of the functional SA axis seen during this period occurs in tandem with similar microstructural refinements. Lifespan trends in structural gradient range (Figure 6d) largely mirror the trends for their functional gradient counterparts, however maximum range of the SA-aligned structural gradient occurs earlier at 9.2 years (95% CI 6.4-11.1 years), suggesting that maximum microstructural differentiation with respect to the SA hierarchy precedes maximal functional differentiation. Similarly, global microstructural gradient dispersion peaks earlier than functional gradient dispersion, reaching its maximal value at 10.2 years (95% CI 4.6-12.4 years). Interestingly, after a period of steady decline in dispersion from 10.2-56 years, we see an increase in structural gradient dispersion for the remainder of the lifespan.

Gradient measures are stable across the lifespan with respect to sex and are hemispherically symmetric. We also sought to identify sex differences in global gradient characteristics by fitting GAMMs to gradient range and dispersion for males and females separately (Figure S7a,c). Notably, we observe higher dispersion and SA gradient range in males across the lifespan, however this difference did not meet the threshold for statistical significance. We also sought to identify

sex-based differences in dispersion by fitting GAMMs analogously with sex treated as a categorical input variable, but we observed no statistically significant differences in lifespan dispersion trajectories with respect to sex. We also fit GAMMs to gradient value at each vertex for males and females separately, and computed the lifespan average difference between the male and female fits, yielding a lifespan average spatial map of sex-based differences in gradient value for each axis (Figure S7b). Interestingly, we observe higher gradient values in the positive pole of the SA axis in the IPL for females than males, but higher values in the positive pole of the MR axis in premotor and control-oriented regions of parietal cortex in males than in females. We further analyzed differences in global gradient measures between the left and right hemisphere by computing gradient range and dispersion for each hemisphere separately and performing GAMM fitting (Figure S8). Notably, gradient range and dispersion curves are nearly identical between hemispheres, indicating that these global hierarchies to not exhibit significant left-right asymmetry across the lifespan.

DISCUSSION

In this work, we studied how multiple fundamental organizing axes of the functional connectome develop from cradle to grave and present the first ever longitudinal atlas of gradient organization that spans the entire human lifespan. Our findings offer abundant novel observations concerning the unfurling and refinement of fundamental axes of the functional organization of the cortex and unify decades of developmental FC research under one comprehensive normative chart of gradient organization. Our work recapitulates previous findings concerning the timing and topographical organization of FC and synthesizes these results under the gradient mapping analysis framework. Integrating the vast and diverse body of fMRI literature into an easily interpreted and succinct framework represents a central obstacle to neuroscience; the present study offers an enormous step forward towards achieving this goal. Finally, the charting of normative developmental trajectories is a critical tenant of modern medicine, allowing for the identification of disease onset and the targeting of early treatment. While cortical morphology has been mapped in detail throughout the human lifespan[47], such charts for the development of FC from days after birth into late old age were sorely lacking until now.

Specifically, we studied the sensory-association, visual-somatosensory, and modulation-representation gradients of functional connectivity, and found that their developmental trajectories are distinct and nonlinear. We first sought to characterize topographic changes in these axes over the lifespan, crucially observing that gradient topography is largely established by 4 years of age. In keeping with previous observations that infant FC architecture is distinct from that of adults[18,28], we observe significantly altered SA and MR gradient topography during early life, indicating weakly developed high-order information processing hierarchies and low levels of the long-range connections that support them. Conversely, the VS axis is fully established during early infancy and its topography remains largely unchanged throughout the remainder of the lifespan, indicating that the distinction between visual and somatosensory unimodal processing is a salient FC organizing motif from cradle to grave.

The SA and MR gradients both enumerate information processing hierarchies crucial to complex cognition, with high-order association and control regions positioned at their apexes,

respectively. We observe similar nonlinear development in gradient range, dispersion, and topographic similarity to the template gradients for the SA and MR axes, indicating that the lifespan development of these transmodal hierarchical axes of organization are interrelated. Despite qualitative similarity in their global development, we observe more protracted maturation of the MR axis compared to the SA axis, indicating that high-order control systems and the global differentiation between modulation and representation is the last major functional organizing motif to develop.

The VS axis undergoes distinct development compared to SA and MR axes, undergoing rapid expansion during infancy, followed by contraction throughout the remainder of the lifespan. The range of the VS axis represents the level of differentiation between primary unimodal processing systems; its increase during infancy reflects functional differentiation of these systems, while its decrease thereafter indicates a continual reduction in the importance of this axis as an organizing motif of the functional connectome. Our observation that the gradient range of the VS axis decreases throughout childhood and adolescence is consistent with previous work[8,48]; however our results differ from these studies in that we do not observe reordering between the SA and VS axes during this period. Importantly, our vertex-wise GAMM estimate of the SA gradient indicates that during infancy and childhood, the somatomotor system occupies the extreme negative pole of the SA axis, suggesting that there is significant "mixing" between the SA and VS axes during this period. Further, in contrast to the SA and MR axes, the cortical locations occupying the poles of the VS axis (visual and somatosensory cortex) are spatially contiguous. The decrease in the range of the VS axis in tandem with the increase in the range of SA and MR axes during development therefor reflect a transition from a locally- to a globally-organized functional connectivity architecture, which is consistent with prior studies[18].

Our analysis of global gradient metrics across the lifespan also yielded several notable results which provide insight into the development of global hierarchical FC architecture. A monotonic increase in dispersion between 5 and 30 years (Figure 3b) indicates that global connectivity differentiation with respect to the SA, VS, and MR axes expands significantly during this period. Declining gradient range of the VS axis during this same period (Figure 3a), however, underscores that the increasing dispersion during this period is driven primarily by expanding transmodal SA and MR axes. It is also notable that increases in gradient dispersion are modest during infancy and early childhood, a developmental stage well-known for rapid differentiation of cortical FC[14,49]. In tandem, expanding gradient range during this period in combination with relatively stable dispersion indicates that the extreme values along each gradient are increasing during this period while not driving a significant change in the average spread of vertices in the embedding space. This trend is potentially explained by increased prominence of transmodal hubs at the positive poles of the SA and MR axes in combination with increasing integration among intermediary and specialized cortical locations. Migration of hubs towards more extreme positions in the embedding space engenders increasing gradient range, while increased integration among intermediary nodes constrains the median global spread (dispersion) of cortical regions. We also observe monotonic decline in global gradient dispersion after 27.7 years (95 % CI 20.0-34.2 years), indicating decreasing FC differentiation during aging. This is consistent with previous observations that FC segregation decreases during later adulthood, while within-system FC and between-system FC decrease and increase, respectively[50,51].

Many previous studies have studied FC organization via graph-theoretic metrics[52–54], while little effort has been made to establish connection between FC gradients and underlying graph architecture. Our analysis sought to partially address this gap by studying the relationship between graph-theoretic metrics, including characteristic path length, and metrics derived from diffusion embedding (DE). We found a particularly interesting relationship between the ratio of the first DE eigenvalue and the sum of all DE eigenvalues ("Eigenvalue Ratio") to characteristic path length, observing a moderate negative correlation ($\rho = -0.27$, $p < 10^{-40}$) across subjects (Figure 3d). Eigenvalue ratio describes the importance of the first diffusion embedding axis relative to all axes, with higher eigenvalue ratios indicating that FC organization is primarily organized along one axis and lower ratios indicating shared importance across multiple axes. Characteristic path length quantifies the average shortest path between vertices in a graph, providing a measure of how interconnected the graph is. We found that increasing characteristic path length tends to correspond to decreasing eigenvalue ratio, indicating that FC graphs with more multi-dimensional architecture (lower eigenvalue ratio) are less interconnected on a global scale. Further, we observe that during infancy, eigenvalue ratio and characteristic path length tend to be low, indicating that infant FC networks have multi-dimensional global architecture and are highly interconnected. This is potentially explained by the high gradient range of the VS axis during this period in combination with a rapidly developing but weakly expressed SA and MR axis. Decreasing eigenvalue ratio during infancy and early childhood (Figure 3e) further illustrate that this period incurs dramatic changes in the dominant organizational axis of FC. Increasing eigenvalue ratio between 2 and 30 years suggest that FC becomes increasingly organized along the SA axis and that global FC architecture becomes increasingly hierarchical during this period. Interestingly, we do not observe a decline in eigenvalue ratio during late adulthood and aging as we do for gradient range of the SA axis. Together, these results suggest that aging incurs a global decrease in FC differentiation rather than the preferential decline of any particular gradient axis.

We also sought to characterize how gradient organization evolves across the human lifespan with respect to resting-state networks (RSNs). We analyzed the trajectories of networks from the well-studied 7 network parcellation of Yeo et al.[44], characterizing the trajectories and distributions of their constituent vertices in our gradient space. These analyses revealed an intricate and complex sequencing of network development with respect to the SA, VS, and MR axes, with differential trajectories across networks and across gradient axes. Network trajectories along the SA and VS axis are simple and understandable. Motion of each network along these axes coincides with changes in SA and VS range, driving expansion and contraction of the separation of networks at either pole. Importantly, there is very little reordering of the position of networks along the SA and VS axes, indicating a relatively low degree of topographic reorganization with respect to these gradients. In contrast, network centroids along the MR axis undergo significant reordering, with differential timing for maturation across networks. This complexity suggests that the MR axis demands significant topographic reorganization of FC throughout development, reaching maturity at the latest stage compared to SA and VS axes. Interestingly, dorsal and ventral attention networks (DAN and VAN) vary significantly in their developmental timing on the MR axis, with the DAN reaching its maximum MR value during late childhood, and the VAN attaining its maximum value during early adulthood. This suggests that during early life, refinement of the top-down attention mechanisms associated with the DAN takes center stage,

with the development of bottom-up attention (VAN) systems playing out over a more protracted period. Further research on the differential development of these two attention systems and their interrelationships may provide further insight to the cognitive significance of these findings.

Several networks undergo opposite developmental trends in mean value on the MR axis. Namely, the DAN and DMN rapidly separate during infancy and childhood, and move to a more central position throughout the remainder of the lifespan. Similarly, the VAN and somatomotor networks are proximal during infancy, and undergo a prolonged period of increasing MR separation through mid adulthood. This is particularly striking, as it indicates that the increasing differentiation between modulation and representation loci is actualized via increasing contrast between the spatially adjacent premotor and ventral attention networks. Further, the prolonged developmental evolution of this abrupt functional development indicates that the development of bottom-up attention and its relationship with primary motor systems continues to mature throughout adulthood, scaffolding a crucial information processing hierarchy.

Our analysis of gradients of cortical morphology and microstructure revealed distinct trajectories for structure-function alignment across the SA, VS, and MR axes. Concomitant increases in structure-function alignment during infancy mark a period of cortical differentiation. A subsequent decrease in alignment for the SA and MR axes during childhood (2–5 years) is potentially reflective of structure-function decoupling driven by increasing functional flexibility and global integration of the transmodal cortices that reside at the apexes of these two processing hierarchies. Conversely, continued increase in structure-function alignment for the VS axis throughout development (birth to 18 years) may reflect increasing domain-specificity and microstructural adaptation of the unimodal cortices.

Limitations, outstanding questions, and future directions. It is important to note that there are many degrees of freedom in our methodology, as the present work is fundamentally exploratory. The use of a template gradient set and the subsequent alignment of individual subject gradients to that template prior to GAMM fitting was crucial to standardizing gradient architecture across the lifespan so that the same characteristics of connectivity could be examined at all ages. However, this implies that there exist global organizational features of connectivity that persist from birth to death. When the template gradient set was computed using gradients from subjects of all ages (including neonates), gradient topography varied significantly, and were less clearly associated with succinct hierarchical properties. The alignment of infant and childhood gradient sets to this adult template yields the best representation of the adult connectivity features present in each infant or child, irrespective of whether those features are principal organizing connectivity motifs. In light of this, our analysis reveals how FC in early life converges towards adult FC with respect to SA, VS, and MR axes, rather than exploring how organizing motifs of FC themselves evolve during early development. Although subtle, this distinction is worth considering and its implications are worth exploring in future studies.

METHODS

Materials. Our subjects were selected from 4 imaging datasets: the Baby Connectome Project (BCP)[55], and the development, young-adult, and aging cohorts of the Human Connectome Project (HCP-D, HCP-YA, HCP-A)[56]. Subjects in the BCP ranged from 16 days to 6 years old, with 276 subjects (126 males, 150 females) scanned at 496 unique timepoints for a total of 1482 scans prior to gradient-based quality control. We used 615 subjects (285 males, 330 females, age 5.58–21.92 years) from the HCP-D, 1008 subjects (458 males, 550 females, age 22–37 years) from the HCP-YA, and 616 subjects (262 males, 354 females, age 36–100 years) from the HCP-A. Across all four cohorts, our dataset included 2,735 subjects (1,131 males, 1,384 females) with median age 26 years and standard deviation of 21.33 years. Cortical surface mesh atlases were constructed for 41 milestone timepoints spanning from birth to 100 years, and individual cortical surface meshes with vertex-to-vertex correspondence were constructed for each subject. For each subject, there were two rs-fMRI sessions, each acquired with 2 phase encoding directions, for a maximum of 4 scans per subject.

Data Preprocessing – Functional MRI. For the BCP dataset, fMRI data was subjected to a thorough infant-specific preprocessing pipeline[57] inspired by the Human Connectome Project (HCP)[13]. This process included head motion correction, EPI distortion correction using FSL's TOPUP, registration to structural MRI T1w image, one-time resampling for efficient mapping to T1w space, high-pass filtering (cutoff = 0.001 Hz) to remove slow drifts, and ICA-AROMA denoising[58] with 150 independent components to eliminate residual motion artifacts. To ensure data quality, we computed framewise displacement (FD) from motion parameters obtained during head motion correction. We excluded samples that exhibit excessive motion, i.e., with a mean Power's FD (absolute sum of motion parameters) exceeding 0.5 mm—a common threshold in fMRI studies[59]. Among 1656 preprocessed fMRI samples, 1493 met the Power's FD criterion. Following this, we visually evaluated skull stripping, tissue segmentation, and fMRI-to-T1w image registration, retaining 1482 samples of satisfactory quality. The BCP fMRI data was mapped to infant-tailored cortical surface meshes[60] with 10,242 vertices per hemisphere using ribbon-constrained volume-to-surface mapping implemented in Connectome Workbench[61].

The fMRI data from HCP-D, YA, and A cohorts were subjected to the HCP minimal preprocessing pipeline[61]. Volumetric fMRI preprocessing steps included correction of gradient-nonlinearity-induced distortion, framewise motion correction using 6 DOF FLIRT registration, phase-encoding distortion correction, and nuisance regression using ICA-FIX. Volumetric fMRI were then mapped to the 32k fs LR mesh[61].

In order to establish a consistent coordinate system across the entire lifespan, we utilized in-house lifespan surface atlases extended from the work of Sahar et al.[60]. The reconstructed cortical surfaces of each individual were first registered to age-matched cortical surface atlases to get vertex-wise correspondence among all the surfaces across the lifespan. Cortical surfaces were mapped onto unit sphere and Spherical Demons[62] was used to perform registration between spherical surfaces of the individuals and the age-matched surface atlases. The vertex-wise correspondence established as a result of spherical registration was then propagated to the white and pial surfaces by leveraging one-to-one correspondence between the spherical and standard representation of the white and pial surfaces. For the HCPD, HCPYA, and HCPA cohorts, we

then resampled fMRI timeseries from the 32k fs LR surface space to our 20k surface space using spherical mapping.

Data Preprocessing – Structural and Diffusion MRI. Structural and diffusion MRI data of the BCP cohort was preprocessed with an in-house baby-centric pipeline[63]. Structural data underwent automated quality assessment[64], inhomogeneity correction, and linear transformation of T2w image to respective T1w image. We then delineated white matter, gray matter, and the cerebrospinal fluid with automated segmentation. Usable diffusion data were selected using a deep-learning based semi-automated QC[65]. Then we performed correction of signal drop-out, pileup, and eddy-current and susceptibility induced distortions using rotation-invariants contrasts of diffusion spherical harmonic images and structural MRI[66]. During this step, we also performed co-registration between dMRI and sMRI using multi-channel non-linear registration with ANTs. Finally, manual visual inspections were done to ensure quality, especially for newborn scans.

Data of the HCP-D, YA, and A cohorts was preprocessed using the HCP preprocessing pipeline[61]. For structural data, processing involved intensity normalization, co-registration, brain extraction, and surface reconstruction. For diffusion data, processing involved eddy-current and susceptibility induced distortions correction, gradient nonlinearity correction, and co-registration with structural data.

Structural and diffusion indices were computed in the same manner for all cohorts. Specifically, cortical thickness is defined as the Euclidean distance between two correspondent vertices on the white and pial surfaces and myelination is quantified using the ratio between T1w and T2w images[67]. Spherical Mean Spectrum Imaging (SMSI)[68,69] was used to calculate intra-cellular volume fraction, extra-cellular volume fraction, intra-soma volume fraction, microscopic fractional anisotropy, microscopic mean diffusivity, microscopic anisotropy index, and orientation coherence index. Diffusion Tensor Imaging (DTI) was used to calculate fractional anisotropy and mean diffusivity.

Gradients. FC matrices were computed from the vertex-wise fMRI timeseries for each acquistion from each subject using the pairwise Pearson correlation coefficient. We then computed the mean FC matrix for each subject, subjected the mean FC matrix to row-wise thresholding (top 10 percent of connections retained), and computed the normalized angle matrix in keeping with previous gradient literature[1,9,25,70]. We computed 20 FC gradients for each subject using the diffusion map embedding implementation in BrainSpace[25] using the normalized angle matrix as the input affinity matrix. In order to achieve correspondence between gradient axes across subjects and age, we computed a set of template gradients by aggregating all individual subject gradients into one large matrix and computing its principal axes of variation using principal component analysis. Next, we aligned the gradient sets of all subjects to this template embedding space using iterative Procrustes alignment[25], after which gradients of the same order were correspondent across all subjects. For quality control, we visually inspected individual subject gradients, and computed key metrics including gradient range and dispersion. Subjects whose principal gradients were dominated by noise as per visual inspection and subjects whose dispersion or gradient ranges were greater than 5 standard deviations away from the lifespan mean of these metrics were excluded from subsequent analyses, leaving 2,735 datapoints.

We also computed cortical gradients based on structural and microstructural features to assess structure-function coupling across the lifespan. Our structural features included 11 measures: cortical thickness, myelination, intra-cellular volume fraction, extra-cellular volume fraction, intra-soma volume fraction, fractional anisotropy, mean diffusivity, microscopic fractional anisotropy, microscopic mean diffusivity, microscopic anisotropy index, and orientation coherence index For each subject, we constructed feature vectors containing these features at each cortical surface vertex, and computed a structural affinity matrix using pairwise Pearson correlation coefficient between structural feature vectors. We then used this affinity matrix as input to the diffusion map embedding algorithm to obtain structural gradients. In order to compare structural and functional gradients across the lifespan, we aligned each subject's structural gradients to that subject's functional gradients, which were previously aligned to the functional template gradients comprised of the SA, VS, and MR axes. All subsequent comparisons between structural and functional gradients were based on these aligned structural gradients.

Generalized Additive Mixed Models (GAMMs). Brain development throughout the lifespan is nonlinear. Further, portions of our dataset utilize longitudinal staggered cohort study design. In light of recent evidence demonstrating the efficacy of GAMMs for estimating lifespan trajectories of biological data[26], we utilized this framework to obtain fits for gradient values and gradient-derived quantities of interest throughout the present study. For all GAMM fits, age was treated as a smooth term, and subject ID and study cohort were treated as random effects. To obtain lifespan trajectories of each gradient of interest, we first fit GAMMs separately for each cortical surface vertex using cubic splines and restricted maximal likelihood approach for smoothing parameters. We assessed fit quality with a range of smooth term basis complexities (k), and observed an optimal adjusted R squared for $k = 4$ for the majority of cortical surface vertices. Further, we extracted the intercept associated with the subject ID and study cohort random effects and applied these intercepts to adjust the underlying data in order to obtain harmonized individual gradients across the lifespan.

We were also interested in lifespan changes in a number of gradient-derived metrics including dispersion, gradient range, and several network-parcellation-based gradient metrics. In each of these cases, metrics of interest were computed based on Procrustes-aligned individual gradients, with population lifespan metric trajectories (e.g., gradient range in Figures 3a–c,e) obtained via GAMM fitting of metric value as a function of age as a smooth term with basis complexities between 3 and 8 spline functions and with subject and cohort IDs as random effects. In several cases, it was of interest to obtain estimates of the age at which gradient-derived metrics reached maxima or minima in their lifespan trajectories as an estimate of their maturation age. To obtain uncertainty estimations for the ages at which each metric reached its maximum or minimum value, we used a bootstrapping procedure. We drew 20,000 samples from the posterior distribution of the smooth term's (age) coefficients, reflecting uncertainty in the model estimates. Each sample represented a possible realization of the age-metric relationship, from which we calculated the fitted metric values across the age sequence. For each bootstrap sample, we identified the age at which the metric achieved its maximum (or minimum) value, thus creating a distribution of ages corresponding to these extreme values across all samples. The 95% high density confidence intervals (CIs) were then computed from this distribution, providing a probabilistic range within which the true age of maximum (or minimum) metric value was most likely to be found.

Visualization. Figure 1 illustrates our analysis framework and aims to establish visualization conventions to facilitate fast and simple interpretations of our lifespan gradients. First, we associate a color-map with each gradient axis. For the SA, VS, and MR axes, these gradient-specific color-maps span from white to red, green to blue, and black to gray, respectively. To visualize the topography of all three gradients on the cortical surface simultaneously, we devised a color-mapping scheme that combines the gradient-specific color maps such that vertices at the apex of the SA axis are red, vertices at the apex of the MR axis are gray, and the visual and somatosensory poles of the VS axis are blue and green, respectively. In Figure 1b, we display 3-dimensional embeddings of all three gradients with our 3-dimensional color-map, and establish notation to indicate embedding axis orientation.

Figure 2a utilizes the aforementioned gradient-specific color-maps to chart topographical progression of each gradient in combination with density plots for gradient value. Importantly, we use a constant range with respect to time for the color-maps of surface-based gradient plots. Density plots are computed using kernel density estimation (KDE) applied to the vertex-wise GAMM prediction of gradient value at selected time points. Prior to density estimation, we normalize gradient values across vertices and all timepoints to range between 0 and 1. To showcase longitudinal changes in both the shape and the scale of density distribution, we use constant horizontal and vertical axis ranges across time.

In Figure 5 (bottom), we display median between-network embedding distance in matrix form, where median distance between each network pair is encoded by the color of that cell.

Gradient Measures. To fully characterize how gradient architecture evolves throughout the human lifespan, we employ and define a number of quantitative measures of their properties. The Euclidean distance between vertices in a diffusion embedding approximates the geodesic distance in the underlying graph from which it was computed. Thus, the Euclidean distance between vertices in our gradient embedding space approximates connectivity differentiation between those vertices. To measure the global degree of FC differentiation in a subject's FC diffusion embedding, we define gradient dispersion as the mean Euclidean distance between the embedding coordinate of all vertices and the centroid of the embedding. For a diffusion embedding with embedding coordinates $\xi_i = (x_i, y_i, z_i)$ for each vertex i where x, y, and z refer to the SA, VS, and MR gradient value, respectively, we define dispersion among N_{vert} vertices as $\sum_{i=1}^{N_{\text{vert}}} |\xi_i - \bar{\xi}| / N_{\text{vert}}$. Within-network dispersion was computed analogously for constituent vertices of each of the 7 RSNs[44].

To characterize the degree of FC differentiation along each gradient axis individually, we compute gradient range. We compute gradient range for each subject and each gradient using the inter-vigintile range (5th percentile to 95th percentile). By using robust statistical measures, we reduce the influence of noise in FC gradients on these global estimates. Gradient range quantifies the degree to which FC is differentiated along a particular gradient axis. Importantly, gradient range is highly correlated with gradient variance (median absolute deviation of gradient value) across subjects (ρ = 0.91, 0.86, 0.89 for SA, VS, and MR axes, respectively), indicating consistent range in the diffusion embedding axes prior to scaling by eigenvalue.

The topographic alignment between individual subject gradients and our template gradient

was of high interest, allowing us to assess both the quality of the Procrustes alignment procedure and the lifespan changes in gradient topography. To assess this similarity, we compute the cosine similarity between individual subject gradients and the corresponding group-level template gradient.

We also analyzed between-network interactions in our gradient embedding space to probe the lifespan trajectories of inter-network coupling. To this end, we devised a principled measure of network-network embedding distance to quantify the degree of FC similarity between different RSNs. Specifically, between-network embedding distances shown in Figure 5 were computed as the median Euclidean distance between all possible vertex pairs from two networks. Network pairs that are highly segregated in the embedding space correspond to large between-network distances, whereas pairs that are integrated or share similar connectivity profiles have low between-network distances.

Supplementary Information The manuscript contains supplementary material.

Author Contributions H.P.T.: methodology, software, investigation, visualization, writing - original draft, writing – review and editing. K.-H.T.: data curation, methodology, software, writing – review and editing. K.M.H.: data curation, methodology, software, writing – review and editing. W.L.: resources. S.A.: resources, methodology, software, writing – review and editing. P.-T.Y.: conceptualization, supervision, funding acquisition, investigation, validation, writing – review and editing.

Data Availability Data used in this study from BCP, HCPD, HCPYA, and HCPA are available from the National Institute of Mental Health Data Archive (NDA, `https://nda.nih.gov`) or by contacting the investigative teams[55,56].

Code Availability Gradient computation and cortical surface visualization were carried out using the BrainSpace toolbox[25]. Volume-to-surface mapping of fMRI timeseries and computation of functional correlation matrices was conducted using Connectome Workbench[71]. Manipulation of FC matrices and computation of gradient-based metrics were carried out in python using standard libraries including Numpy[72], Scipy[73], and Sci-Kit Learn[74]. Manipulation of neuroimaging-specific file types was carried out using Nibabel[75]. GAMM fitting was carried out with the MCGV R package[76], while visualization of lifespan curves and data manipulation in R was carried out using the Tidyverse R libraries[77].

Acknowledgements This work was supported in part by the United States National Institutes of Health (NIH) through grants R01 MH125479 and R01 EB008374.

Competing Interests The authors declare that they have no competing financial interests.

Correspondence Correspondence and requests for materials should be addressed to P.-T.Y.

1. Margulies, D. S. *et al.* Situating the default-mode network along a principal gradient of macroscale cortical organization. *Proceedings of the National Academy of Sciences of the United States of America* **113**, 12574–12579 (2016).

2. Huntenburg, J. M., Bazin, P. L. & Margulies, D. S. Large-scale gradients in human cortical organization. *Trends in Cognitive Sciences* (2018).

3. Parkes, L., Satterthwaite, T. D. & Bassett, D. S. Towards precise resting-state fmri biomarkers in psychiatry: synthesizing developments in transdiagnostic research, dimensional models of psychopathology, and normative neurodevelopment. *Current Opinion in Neurobiology* **65**, 120–128 (2020).

4. Sporns, O. Graph theory methods: Applications in brain networks. *Dialogues in Clinical Neuroscience* **20**, 111–120 (2018).

5. Smallwood, J. *et al.* The default mode network in cognition: a topographical perspective. *Nature Reviews Neuroscience* **22**, 503–513 (2021).

6. Zhang, J. *et al.* Intrinsic functional connectivity is organized as three interdependent gradients. *Scientific Reports* (2019).

7. Moore, J. W. *et al.* Gradient organisation of functional connectivity within resting state networks is present from 25 weeks gestation in the human fetal brain. *eLife* (2023).

8. Xia, Y. *et al.* Development of functional connectome gradients during childhood and adolescence. *Science Bulletin* **67**, 1049–1061 (2022).

9. Bethlehem, R. A. *et al.* Dispersion of functional gradients across the adult lifespan. *NeuroImage* **222**, 117299 (2020).

10. Fan, Y. *et al.* Brain anatomical networks in early human brain development. *NeuroImage* (2011).

11. Ball, G. *et al.* Rich-club organization of the newborn human brain. *Proceedings of the National Academy of Sciences of the United States of America* **111**, 7456–7461 (2014).

12. Gao, W. *et al.* Evidence on the emergence of the brain's default network from 2-week-old to 2-year-old healthy pediatric subjects. *Proceedings of the National Academy of Sciences of the United States of America* (2009).

13. Zhang, H., Shen, D. & Lin, W. Resting-state functional MRI studies on infant brains: A decade of gap-filling efforts. *NeuroImage* **185**, 664–684 (2019).

14. Gao, W., Alcauter, S., Smith, J. K., Gilmore, J. H. & Lin, W. Development of human brain cortical network architecture during infancy. *Brain Structure and Function* (2015).

15. Wang, R. *et al.* Segregation, integration, and balance of large-scale resting brain networks configure different cognitive abilities. *Proceedings of the National Academy of Sciences of the United States of America* (2021).

16. Whitaker, K. J. *et al.* Adolescence is associated with genomically patterned consolidation of the hubs of the human brain connectome. *Proceedings of the National Academy of Sciences of the United States of America* (2016).

17. Park, B. Y. *et al.* An expanding manifold in transmodal regions characterizes adolescent reconfiguration of structural connectome organization. *eLife* (2021).

18. Fair, D. A. *et al.* Functional brain networks develop from a "local to distributed" organization. *PLoS Computational Biology* (2009).

19. Luna, B., Padmanabhan, A. & O'Hearn, K. What has fMRI told us about the development of cognitive control through adolescence? *Brain and Cognition* (2010).

20. Baum, G. L. *et al.* Modular segregation of structural brain networks supports the development of executive function in youth. *Current Biology* **27**, 1561–1572 (2017).

21. Wendelken, C., Ferrer, E., Whitaker, K. J. & Bunge, S. A. Fronto-parietal network reconfiguration supports the development of reasoning ability. *Cerebral Cortex* (2016).

22. Geerligs, L., Renken, R. J., Saliasi, E., Maurits, N. M. & Lorist, M. M. A brain-wide study of age-related changes in functional connectivity. *Cerebral Cortex* (2015).

23. Egimendia, A. *et al.* Aging reduces the functional brain networks strength—a resting state fMRI study of healthy mouse brain. *Frontiers in Aging Neuroscience* (2019).

24. Heckner, M. K. *et al.* The aging brain and executive functions revisited: Implications from meta-analytic and functional-connectivity evidence. *Journal of Cognitive Neuroscience* (2021).

25. Vos de Wael, R. *et al.* BrainSpace: a toolbox for the analysis of macroscale gradients in neuroimaging and connectomics datasets. *Communications Biology* (2020).

26. Chen, C. Generalized additive mixed models. *Communications in Statistics - Theory and Methods* **29**, 1257–1271 (2000).

27. Nazari, R. & Salehi, M. Early development of the functional brain network in newborns. *Brain Structure and Function* (2023).

28. Yin, W. *et al.* The emergence of a functionally flexible brain during early infancy. *Proceedings of the National Academy of Sciences of the United States of America* (2020).

29. Larivière, S. *et al.* Multiscale structure-function gradients in the neonatal connectome. *Cerebral Cortex* **30**, 47–58 (2020).

30. Schaefer, A. *et al.* Local-global parcellation of the human cerebral cortex from intrinsic functional connectivity MRI. *Cerebral Cortex* (2018).

31. Supekar, K., Musen, M. & Menon, V. Development of large-scale functional brain networks in children. *PLoS Biology* (2009).

32. Keller, A. S. *et al.* Hierarchical functional system development supports executive function. *Trends in Cognitive Sciences* 1–15 (2022).

33. Power, J. D. & Petersen, S. E. Control-related systems in the human brain. *Current Opinion in Neurobiology* (2013).

34. Parlatini, V. *et al.* Functional segregation and integration within fronto-parietal networks. *NeuroImage* (2017).

35. Pozuelos, J. P., Paz-Alonso, P. M., Castillo, A., Fuentes, L. J. & Rueda, M. R. Development of attention networks and their interactions in childhood. *Developmental Psychology* **50**, 2405–2415 (2014).

36. Abrol, A. *et al.* Developmental and aging resting functional magnetic resonance imaging brain state adaptations in adolescents and adults: A large n (>47k) study. *Human Brain Mapping* **44**, 2158–2175 (2023).

37. Sydnor, V. J. *et al.* Intrinsic activity develops along a sensorimotor-association cortical axis in youth. *Nature Neuroscience* **26**, 638–649 (2022).

38. Fair, D. A. *et al.* Development of distinct control networks through segregation and integration. *Proceedings of the National Academy of Sciences of the United States of America* (2007).

39. Vogel, A. C., Power, J. D., Petersen, S. E. & Schlaggar, B. L. Development of the brain's functional network architecture. *Neuropsychology Review* **20**, 362–375 (2010).

40. Rubinov, M. & Sporns, O. Complex network measures of brain connectivity: Uses and interpretations. *NeuroImage* **52**, 1059–1069 (2010).

41. Katsumi, Y. *et al.* Correspondence of functional connectivity gradients across human isocortex, cerebellum, and hippocampus. *Communications Biology* **6**, 1–13 (2023).

42. Casey, B. J., Tottenham, N., Liston, C. & Durston, S. Imaging the developing brain: What have we learned about cognitive development? *Trends in Cognitive Sciences* (2005).

43. Menon, V. Developmental pathways to functional brain networks: Emerging principles. *Trends in Cognitive Sciences* (2013).

44. Thomas Yeo, B. T. *et al.* The organization of the human cerebral cortex estimated by intrinsic functional connectivity. *Journal of Neurophysiology* (2011).

45. Huttenlocher, P. R. & Dabholkar, A. S. Regional differences in synaptogenesis in human cerebral cortex. *Journal of Comparative Neurology* (1997).

46. Petanjek, Z. *et al.* Extraordinary neoteny of synaptic spines in the human prefrontal cortex. *Proceedings of the National Academy of Sciences of the United States of America* (2011).

47. Bethlehem, R. A. I. *et al.* Brain charts for the human lifespan. *Nature* **604**, 525–533 (2022).

48. Holmes, A. J., Dong, H. M., Margulies, D. S. & Zuo, X. N. Shifting gradients of macroscale cortical organization mark the transition from childhood to adolescence. *Proceedings of the National Academy of Sciences of the United States of America* (2021).

49. Wen, X. *et al.* First-year development of modules and hubs in infant brain functional networks. *NeuroImage* (2019).

50. Chan, M. Y., Park, D. C., Savalia, N. K., Petersen, S. E. & Wig, G. S. Decreased segregation of brain systems across the healthy adult lifespan. *Proceedings of the National Academy of Sciences of the United States of America* (2014).

51. Betzel, R. F. *et al.* Changes in structural and functional connectivity among resting-state networks across the human lifespan. *NeuroImage* **102**, 345–357 (2014).

52. van den Heuvel, M. P. & Sporns, O. Network hubs in the human brain. *Trends in Cognitive Sciences* **17**, 683–696 (2013).

53. Sporns, O. & Betzel, R. F. Modular brain networks. *Annual Review of Psychology* (2016).

54. Bassett, D. S. & Bullmore, E. T. Small-world brain networks revisited. *Neuroscientist* **23**, 499–516 (2017).

55. Howell, B. R. *et al.* The UNC/UMN baby connectome project (BCP): An overview of the study design and protocol development. *NeuroImage* (2019).

56. Harms, M. P. *et al.* Extending the human connectome project across ages: Imaging protocols for the lifespan development and aging projects. *NeuroImage* (2018).

57. Thung, K.-H., Wu, Z., Wang, L., Lin, W. & Yap, P.-T. Analysis of ICA-AROMA motion denoising on fMRI data in infant cohort. In *Annual Meeting of the Organization for Human Brain Mapping (OHBM)* (2022).

58. Pruim, R. H. *et al.* ICA-AROMA: A robust ICA-based strategy for removing motion artifacts from fMRI data. *NeuroImage* **112**, 267–277 (2015).

59. Power, J. D., Barnes, K. A., Snyder, A. Z., Schlaggar, B. L. & Petersen, S. E. Spurious but systematic correlations in functional connectivity MRI networks arise from subject motion. *NeuroImage* **59**, 2142–2154 (2012).

60. Ahmad, S. *et al.* Multifaceted atlases of the human brain in its infancy. *Nature Methods* **20**, 55–64 (2023).

61. Glasser, M. F. *et al.* The minimal preprocessing pipelines for the human connectome project. *NeuroImage* (2013).

62. Yeo, B. *et al.* Spherical demons: Fast diffeomorphic landmark-free surface registration. *IEEE Transactions on Medical Imaging* **29**, 650–668 (2010).

63. Ye, W. *et al.* An automated processing pipeline for diffusion MRI in the baby connectome project. In *Annual Meeting of the International Society for Magnetic Resonance in Medicine (ISMRM)* (2021).

64. Liu, S. *et al.* Learning MRI artefact removal with unpaired data. *Nature Machine Intelligence* **3**, 60–67 (2021).

65. Liu, S. *et al.* Multi-stage image quality assessment of diffusion MRI via semi-supervised nonlocal residual networks. In *Medical Image Computing and Computer Assisted Intervention (MICCAI)*, 521–528 (Springer, 2019).

66. Ahmad, S. *et al.* Fast correction of eddy-current and susceptibility-induced distortions using rotation-invariant contrasts. In *Medical Image Computing and Computer-Assisted Intervention (MICCAI)*, 34–43 (Springer, 2020).

67. Glasser, M. F. & Van Essen, D. C. Mapping human cortical areas in vivo based on myelin content as revealed by T1-and T2-weighted MRI. *Journal of Neuroscience* **31**, 11597–11616 (2011).

68. Huynh, K. M. *et al.* Probing tissue microarchitecture of the baby brain via spherical mean spectrum imaging. *IEEE Transactions on Medical Imaging* 1–1 (2020).

69. Huynh, K. M., Wu, Y., Ahmad, S. & Yap, P.-T. Microstructure fingerprinting for heterogeneously oriented tissue microenvironments. In *Medical Image Computing and Computer-Assisted Intervention (MICCAI)* (Springer, 2023).

70. Paquola, C. *et al.* Microstructural and functional gradients are increasingly dissociated in transmodal cortices. *PLoS Biology* (2019).

71. Marcus, D. S. *et al.* Informatics and data mining tools and strategies for the human connectome project. *Frontiers in Neuroinformatics* **5** (2011).

72. Harris, C. R. *et al.* Array programming with NumPy. *Nature* **585**, 357–362 (2020). URL `https://doi.org/10.1038/s41586-020-2649-2`.

73. Virtanen, P. *et al.* SciPy 1.0: Fundamental Algorithms for Scientific Computing in Python. *Nature Methods* **17**, 261–272 (2020).

74. Pedregosa, F. *et al.* Scikit-learn: Machine learning in Python. *Journal of Machine Learning Research* **12**, 2825–2830 (2011).

75. Brett, M. *et al.* nipy/nibabel: 5.2.1 (2024). URL `https://doi.org/10.5281/zenodo.10714563`.

76. Wood, S. *Generalized Additive Models: An Introduction with R* (Chapman and Hall/CRC, 2017), 2 edn.

77. Wickham, H. *et al.* Welcome to the tidyverse. *Journal of Open Source Software* **4**, 1686 (2019).